

Article

# A IR-Femtosecond Laser Hybrid Sensor to Measure the Thermal Expansion and Thermo-Optical Coefficient of Silica-Based FBG at High Temperatures

Litong Li <sup>1,\*</sup>, Dajuan Lv <sup>1,2</sup>, Minghong Yang <sup>2,\*</sup>, Liangming Xiong <sup>1</sup> and Jie Luo <sup>1</sup>

<sup>1</sup> State Key Laboratory of Optical Fiber and Cable Manufacture Technology, Yangtze Optical Fibre and Cable Joint Stock Limited Company, Wuhan 430073, China; lvdajuan@yofc.com (D.L.); xiongliangming@yofc.com (L.X.); luojie@yofc.com (J.L.)

<sup>2</sup> National Engineering Laboratory for Fiber Optic Sensing Technology, Wuhan University of Technology, Wuhan 430070, China

\* Correspondence: 13163386978@163.com (L.L.); minghong.yang@whut.edu.cn (M.Y.); Tel.: +131-6338-6978 (L.L.)

Received: 21 November 2017; Accepted: 17 January 2018; Published: 26 January 2018

**Abstract:** In this paper, a hybrid sensor was fabricated using a IR-femtosecond laser to measure the thermal expansion and thermo-optical coefficient of silica-based fiber Bragg gratings (FBGs). The hybrid sensor was composed of an inline fiber Fabry-Perot interferometer (FFPI) cavity and a type-II FBG. Experiment results showed that the type-II FBG had three high reflectivity resonances in the wavelength ranging from 1100 to 1600 nm, showing the peaks in 1.1, 1.3 and 1.5  $\mu\text{m}$ , respectively. The thermal expansion and thermo-optical coefficient (1.3  $\mu\text{m}$ , 1.5  $\mu\text{m}$ ) of silica-based FBG, under temperatures ranging from 30 to 1100  $^{\circ}\text{C}$ , had been simultaneously calculated by measuring the wavelength of the type-II FBG and FFPI cavity length.

**Keywords:** fiber optics sensor; IR-femtosecond laser; high temperatures; thermal expansion coefficient; thermo-optical coefficient

## 1. Introduction

Fiber Bragg gratings (FBGs) are becoming increasingly important in high temperature application fields such as aerospace engineering, chemical aggressive and energy fields, due to their light weight, immunity to electromagnetic interference, durability against harsh environments, and fast response [1,2]. The induced local material changes in silica fiber yield an increase of the refractive index. FBGs are defined as type-I or type-II depending on whether the exposure intensity is lower or higher than the fiber material damage threshold [3]. However, the long-term instability under high temperature (up to 400  $^{\circ}\text{C}$ ) has limited applications of type-I FBG in the high temperature field.

In recent years, special FBG types such as type-II fiber grating, regenerated fiber grating (RFBG) and sapphire fiber grating (SFBG) have become hot research topics because of their performance at high temperature (higher than 400  $^{\circ}\text{C}$ ) [4–8]. In 2012, the temperature and strain characterizations of seed and regenerated gratings with and without post-annealing was tested under the temperature of 1100  $^{\circ}\text{C}$  [9]. In 2015, sapphire fiber FBGs for high temperature applications were studied up to 1900  $^{\circ}\text{C}$  [10]. In 2016, the type-II gratings within silica suspended-core microstructure optical fibers fabricated by femtosecond lasers were tested at temperatures up to 1300  $^{\circ}\text{C}$  [11]. However, some of these FBGs still have certain limitations, such as the inscription difficulty of SFBGs, and the frangibility and low reflection intensity of RFBGs after repeated annealing. Therefore, researchers have focused on silica-based type-II fiber gratings in recent years.

In previous studies [5,8], theoretical research showed that the wavelength shift of type-II FBGs was mainly determined by the elastic coefficient, thermal expansion coefficient (CTE) and thermo-optical

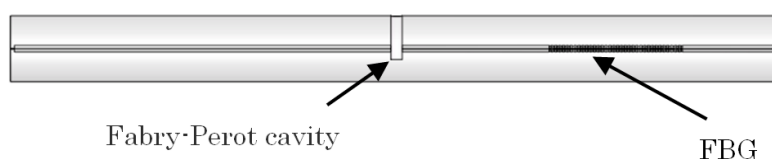
coefficient (TOC). However, the correlation coefficients of silica-based FBGs would no longer be constant at high temperatures, and the known sensing parameters were no longer viable in this situation. Meanwhile, calibration of FBG sensors at high temperatures before any measurements remains an unsolved problem.

Therefore, how to measure the CTE and TOC of silica-based FBGs at high temperatures is an attractive research topic. The traditional measurement method for the TOC and CTE of transparent materials is the prism method [12]. Domenegueti et al. developed a single arm double interferometer for the simultaneous measurement of linear TOC and CTE of solid (silica, BK7, SF6) and liquid (water, ethanol and acetone) samples [13]. Li et al. used an approximately 8-layer graphene diaphragm to fabricate an optical fiber extrinsic FP interferometric sensor which could measure the CTE of a graphene diaphragm [14]. In previous work, we demonstrated a hybrid sensor fabricated by an etching method to measure the CTE and thermo-optical coefficient of silica-based type-I FBG in the temperature range of 30–273 K [15]. However, little research has been done on the temperature coefficient measurement of type-II silica-based FBGs at ultrahigh temperatures.

In this work, we successfully obtained the CTE and TOC of type-II FBGs through a FFPI-FBG hybrid sensor, which was fabricated by infrared (IR) femtosecond (fs) laser micromachining and pulsed radiation with a phase mask. The CTE and TOC of silica-based FBGs has been simultaneously calculated by measuring the wavelength of a type-II FBG and FFPI cavity length. The data accuracy has been carefully examined by comparing with the relevant references

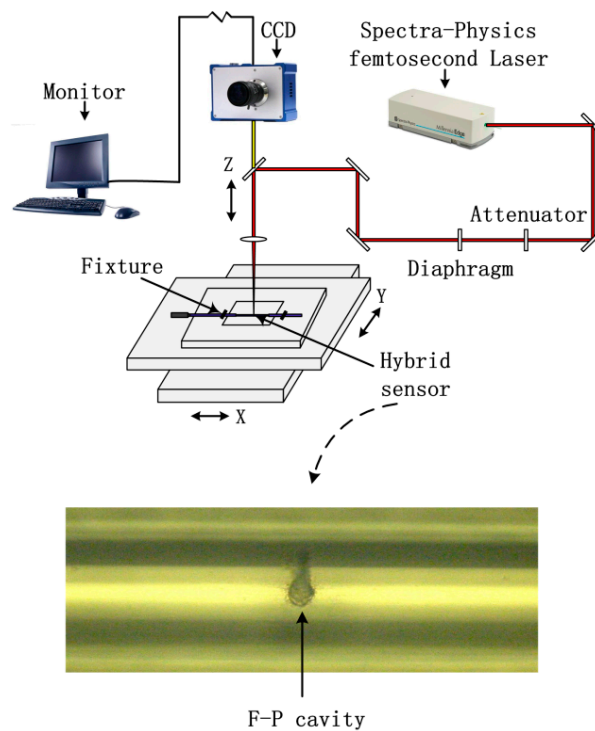
## 2. Principle and Structure of the Sensor

Figure 1 shows the schematic structure of the hybrid sensor. It is composed of an inline FFPI cavity and a type-II FBG.



**Figure 1.** Schematic structure of the FFPI-FBG hybrid sensor.

As shown in Figure 2, the inline FFPI and type-II FBG were both fabricated by a fs laser 3D micromachining system which was composed of four parts, a fs laser (Spectra-Physics Inc., Santa Clara, CA, USA), external optical path, CCD monitoring system (SigamaKoki Inc., Tokyo, Japan) and 3D working platform (Newport Inc., Franklin, MA, USA). The single-mode fiber (SMF) was fused silica HIPOSH<sup>®</sup> fiber (YOFC Ltd., Wuhan, China, with core/cladding of 9  $\mu\text{m}$ /125  $\mu\text{m}$ ). The pulse width and repetition rate of the fs laser were 120 fs and 1 kHz, respectively. The 3D working platform had a movement range of  $\pm 100 \pm 100 \pm 25$  mm (in the X,Y,Z directions, respectively) and the movement accuracy was 1  $\mu\text{m}$ . The pulse energy was controlled by a tunable attenuator. The FBG inscription by the fs laser is a nonlinear and multiphotonic process for optical fibers [16]. The spectra of type-II FBGs was measured by using a supercontinuum source (YSL Photonics Inc., Wuhan, China) with an output wavelength range from 1100 nm to 1600 nm and an optical spectrum analyzer (OSA) (Yokogawa Inc., Tokyo, Japan) with resolution of 0.02 nm. Figure 3 shows that the type-II FBG had three high reflectivity resonances in the wavelength range from 1100 to 1600 nm. The FWHM of the FBG for all three orders (1.1  $\mu\text{m}$ , 1.3  $\mu\text{m}$  1.5  $\mu\text{m}$ ) were 2.58 nm, 1.82 nm, and 0.84 nm, respectively. The pulses used for type-II FBG inscription were 3 mm radius, with 0.6 mJ pulse energy at 1000 Hz repetition rate. The average light power intensity in the focal line was about  $10^{13}$  W/cm<sup>2</sup>. The pulses used for FFPI ablation were 3 mm radius, with 0.8 mJ pulse energy at 100 Hz repetition rate. The laser focusing mode has also been changed from line mode to point mode.



**Figure 2.** Schematic structure of the femtosecond laser 3D micromachining system and the digital microscope image of FP cavity fabricated.

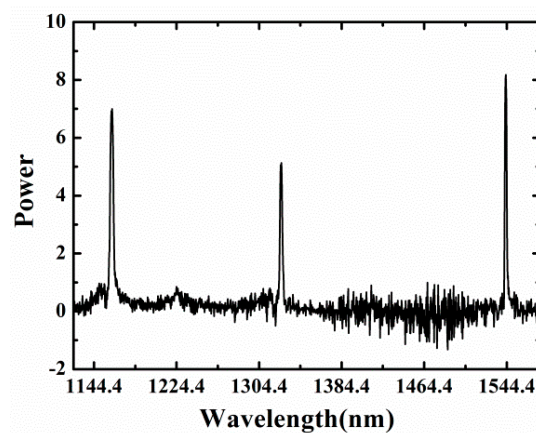


**Figure 3.** High-order spectra of the type-II Bragg grating structure.

Through the cooperation of the 3D platform, the micro-machining of FFPI cavity was carried out around the type-II FBG. It could be seen from the digital microscope (VHX-100) that the interface of the FFPI cavity made by fs laser was coarse and irregular (Figure 2). Then a discharge arc was used to make the cavity interface clean and flat with a fusion splicer (Fujikura Inc., Tokyo, Japan).

Figure 4 showed the transmission spectrum (1.5  $\mu\text{m}$ ) of the hybrid sensor. The wavelength shifts of transmission spectra (1.5  $\mu\text{m}$ ) were recorded by a self-manufactured optical spectrum demodulation (OSD) system (Bayspec Inc., San Jose, CA, USA), in which the acquisition rate was 8 kHz and wavelength resolution was 0.1 pm. The spectral period change of FFPI was mainly determined by the micro-cavity length. The wavelength of the FBG and the cavity of the FFPI would change with the increase of environment temperature.

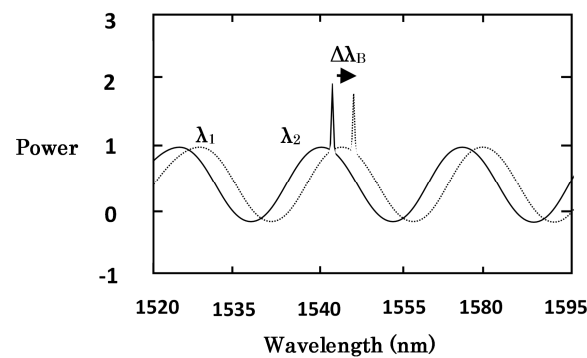


**Figure 4.** Transmission spectrum (1.5  $\mu\text{m}$ ) of the hybrid FFPI-FBG sensor.

The Bragg resonance shift  $\Delta\lambda_{(B,m)}$  equation of the high order type-II FBG could be expressed as:

$$\frac{\Delta\lambda_{(B,m)}}{\lambda_{(B,m)}} = (\zeta + \alpha_m) \times \Delta T \quad (1)$$

where  $\lambda_{(B,m)}$  was the center wavelength of FBG,  $m$  was the diffracted order,  $\zeta$  was the CTE,  $\alpha_m$  was the TOC of the fiber grating at the wavelength  $\lambda_{(B,m)}$ ,  $\Delta T$  meant the variation of temperature.

Where  $\lambda_1$  and  $\lambda_2$  were the wavelength at the two adjacent peaks of the interference fringes [17]. The cavity length  $L$  of the FFPI could be calculated as:

$$L = \frac{\lambda_1 \lambda_2}{2(\lambda_2 - \lambda_1)} \quad (2)$$

The cavity variation  $\Delta L$  could be obtained by the Equation (2) since the temperature change, so the CTE in different range could be expressed by:

$$\zeta = \frac{\Delta L}{L \Delta T} \quad (3)$$

The CTE measured by FFPI was the CTE of the fiber cladding since the fiber core was etched. The main raw material of SMF (YOFC HIPOSH<sup>®</sup> fiber) was fused silica and the material composition and structure in SMF was SiO<sub>2</sub>-GeO<sub>2</sub>-F. Normally only GeO<sub>2</sub> was doped in the central core and only F in the cladding. For PCVD optical fiber, F could be introduced in the core to reduce the water peak. The optical fiber was a cylindrical structure, with a 9  $\mu\text{m}$  diameter core, surrounded by a cladding with 125  $\mu\text{m}$  diameter. The dopant concentrations must be very tiny (nearly 0.1%) to get the perfect viscosity match between the core and cladding. Because the raw material was consistent and doping amount was very tiny, combined with good manufacturing process, the CTEs of the core and cladding could be regarded as approximately the same [18].

Thus the TOC could be expressed as:

$$\alpha_m = \frac{\Delta\lambda_{(B,m)}}{\lambda_{(B,m)} \Delta T} - \zeta. \quad (4)$$

The TOC of silica-based FBG was the effective thermo-optic coefficient of the modes, was different from the TOC of the fiber material.

### 3. Experiment

The schematic setup of the high temperature experiment was shown in Figure 5. Three FFPI-FBG hybrid sensors were placed close to the thermocouple in a tubular calibration furnace (OTF-1200X, KEJING Ltd., Changzhou, China).

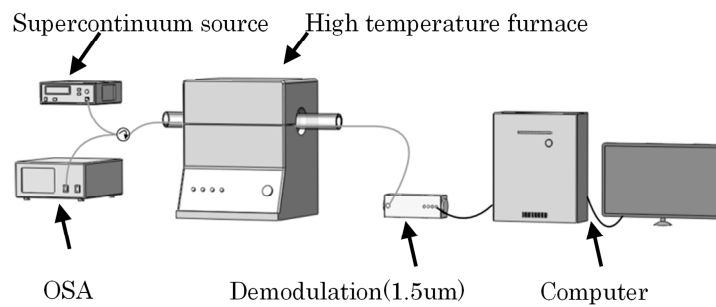


Figure 5. High temperature experimental set-up.

The tubular calibration furnace adopted PID controls with a temperature precision of  $1\text{ }^{\circ}\text{C}$  and had a maximum temperature of  $1200\text{ }^{\circ}\text{C}$ . The thermocouple near the hybrid sensors was used as a reference and for the standard temperature measurement. During the test, the furnace tube was in a vacuum state to avoid the influence of air.

The wavelength shift of resonance in  $1.3\text{ }\mu\text{m}$  of type-II FBG was recorded by an OSA (Yokogawa Inc.). The supercontinuum source and OSA were connected to the two input ports of a 3 dB fiber coupler respectively. One end of the hybrid sensor in the furnace tube was connected to the output port of the coupler and the other end of the hybrid sensor was connected to a self-manufactured OSD (Bayspec Inc.). The temperature started from  $30$  to  $50\text{ }^{\circ}\text{C}$ , then rose to  $1100\text{ }^{\circ}\text{C}$  with a step of  $50\text{ }^{\circ}\text{C}$  and the speed of  $10\text{ }^{\circ}\text{C}/\text{min}$ . In each setting temperature point, the temperature was holding 20 min to ensure the heat exchange and eliminated the influence of the temperature fluctuation.

The high temperature response of the type-II FBG and FFPI are plotted in Figure 6, respectively. The results showed that shift in Bragg wavelengths was nonlinear from  $30$  to  $1100\text{ }^{\circ}\text{C}$ , and the cavity length change was also nonlinear from  $30$  to  $700\text{ }^{\circ}\text{C}$ . The data at the temperature of  $30\text{ }^{\circ}\text{C}$  was defined as the initial values. The initial values of type-II FBGs were ( $1543.6734\text{ nm}$ ,  $1325.56\text{ nm}$ ), ( $1543.3413\text{ nm}$ ,  $1325.272\text{ nm}$ ), and ( $1543.8212\text{ nm}$ ,  $1325.691\text{ nm}$ ), respectively. Also the initial cavity lengths of FFPI were  $63.3994\text{ }\mu\text{m}$ ,  $71.3354\text{ }\mu\text{m}$ , and  $69.1103\text{ }\mu\text{m}$ , respectively. The test temperature was holding 4 h at  $1100\text{ }^{\circ}\text{C}$  and the reflection spectra of the three type-II FBGs did not change throughout the testing process. The peak intensity of the three FFPI data was declined from nearly  $-53\text{ dBm}$  to  $-70\text{ dBm}$  when the temperature exceeds  $700\text{ }^{\circ}\text{C}$ . The OSD was unable to complete the peak search. The FFPI cavity data could hardly keep stable and fluctuated within a dozen microns. This phenomenon could be attributed to the uneven surface of the FP micro-cavity that led to an irregular expansion at such high temperatures, leading to larger intensity loss.

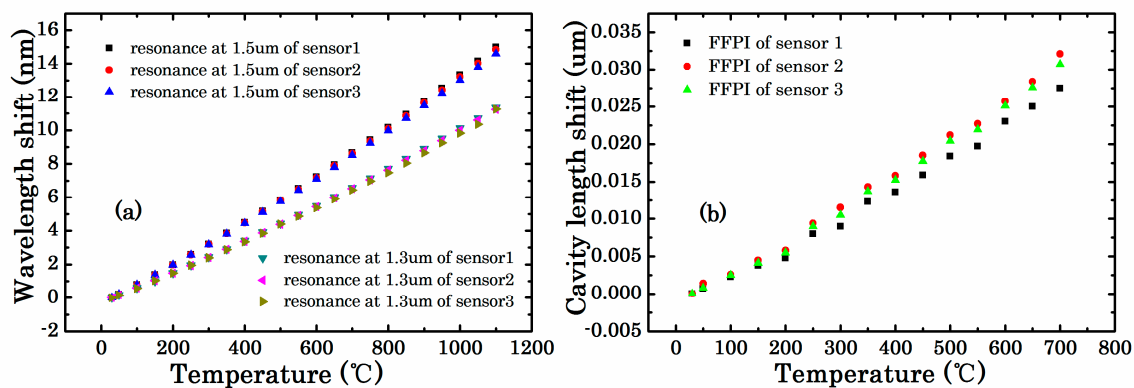
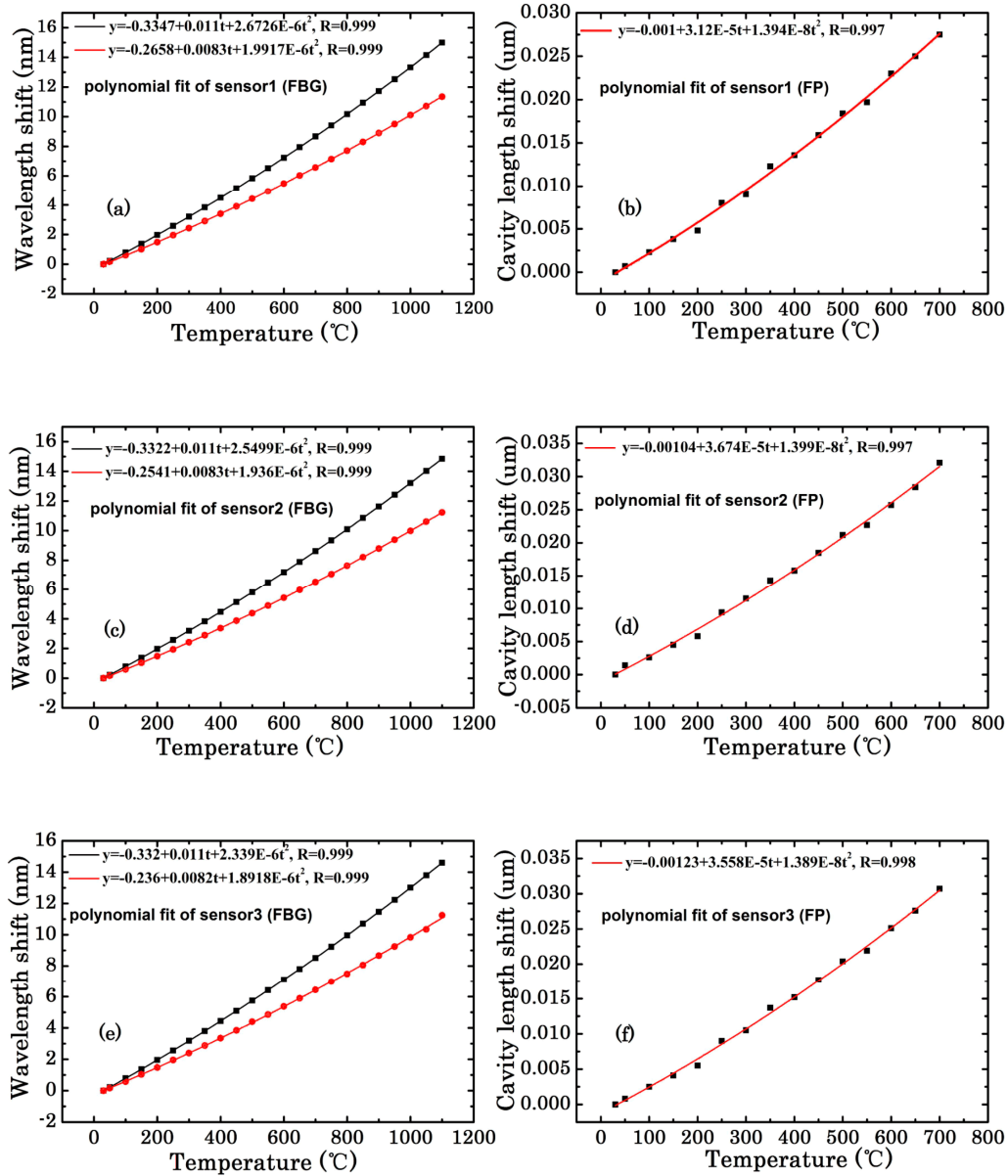


Figure 6. (a) Bragg wavelength shift and (b) FFPI cavity length change versus temperature at high temperatures.

#### 4. Results and Discussion

The dotted lines in Figure 7 are the quadratic polynomial fit curves of the Bragg wavelength and FPPI cavity length changes at different temperatures, respectively.



**Figure 7.** The quadratic polynomial fit curves of Bragg wavelength change versus temperature (a) FBG 1 (c) FBG 2 (e) FBG 3 and FPPI cavity length change versus temperature (b) FP1 (d) FP2 (f) FP3.

For the type-II FBG at the temperature ranging from 30 to 1100 °C, the polynomial expressions were as follows:

$$\Delta\lambda_{(1.5\mu m,1)} = -0.3347 + 0.011T + 2.6726E - 6T^2, \quad (5)$$

$$\Delta\lambda_{(1.5\mu m,2)} = -0.3322 + 0.011T + 2.5499E - 6T^2, \quad (6)$$

$$\Delta\lambda_{(1.5\mu m,3)} = -0.332 + 0.011T + 2.339E - 6T^2, \quad (7)$$

$$\Delta\lambda_{(1.3\mu m,1)} = -0.2658 + 0.0083T + 1.9917E - 6T^2, \quad (8)$$



$$\Delta\lambda_{(1.3\mu\text{m},2)} = -0.2541 + 0.0083T + 1.936E - 6T^2, \quad (9)$$

$$\Delta\lambda_{(1.3\mu\text{m},3)} = -0.236 + 0.0082T + 1.8918E - 6T^2. \quad (10)$$

For the FFPI at the temperature ranging from 30 to 700 °C:

$$\Delta L_1 = -0.001 + 3.12E - 5T + 1.394E - 8T^2, \quad (11)$$

$$\Delta L_2 = -0.00104 + 3.674E - 5T + 1.399E - 8T^2, \quad (12)$$

$$\Delta L_3 = -0.00123 + 3.558E - 5T + 1.389E - 8T^2, \quad (13)$$

where  $T$  was in Celsius.

By differentiating Equation (3) and the average calculation of Equations (11)–(13), the CTE could be given by:

$$\xi = \frac{\Delta L}{L\Delta T} = (0.0041T + 5.07)E - 7. \quad (14)$$

When the temperature was between 30 and 700 °C, the relationship between the CTE and temperature could be described as a linear curve. Differentiating Equation (1) and the average calculation of Equation (5) to Equation (10), the TOC and CTE could be deduced corresponding to the equation as follows:

$$(\alpha + \xi)_{1.5\mu\text{m}} = \frac{\Delta\lambda_B}{\lambda_B\Delta T} = (0.00326T + 7.12)E - 6, \quad (15)$$

$$(\alpha + \xi)_{1.3\mu\text{m}} = \frac{\Delta\lambda_B}{\lambda_B\Delta T} = (0.00292T + 6.23)E - 6. \quad (16)$$

Thus, the TOC could be acquired from Equation (4):

$$\alpha_{1.5\mu\text{m}} = (0.00285T + 6.61)E - 6, \quad (17)$$

$$\alpha_{1.3\mu\text{m}} = (0.00251T + 5.723)E - 6, \quad (18)$$

where  $T$  was in Celsius and temperature was between 30 °C and 700 °C. The relationship between the TOC and temperature also could be described by a linear curve.

When the temperature was between 30 °C and 100 °C, the CTE was between  $5.19 \times 10^{-7}/^\circ\text{C}$  and  $5.48 \times 10^{-7}/^\circ\text{C}$ , TOC  $\alpha_{1.5\mu\text{m}}$  was between  $6.69 \times 10^{-6}/^\circ\text{C}$  and  $6.89 \times 10^{-6}/^\circ\text{C}$ , and  $\alpha_{1.3\mu\text{m}}$  was between  $5.8 \times 10^{-6}/^\circ\text{C}$  and  $5.97 \times 10^{-6}/^\circ\text{C}$ , which agreed well with the theoretical values at room temperature [19–21]. Thus, the curve equation could be used for silica-based FBG standardization procedures at high temperatures. Combined with metal coating technology, it strongly indicated that such a hybrid sensor also had great potential in characterizing the CTE of related metal at high temperatures. A metal coating (gold, copper) could be sputtered on the surface of bare SMF, using the ultrahigh vacuum magnetron sputter system. The thickness of the metal film would be larger than 10  $\mu\text{m}$  and it would distribute homogeneously on the fiber surface. Then femtosecond laser processing could be employed to ablate the FFPI on the metal-coated fiber. The CTE of  $\text{SiO}_2$  was much less than that of metal, so one could calculate the CTE of the coated metal through the FFPI cavity changes.

## 5. Conclusions

The CTE and TOC of silica-based type-II FBGs have been tested by using a hybrid FFPI-FBG sensor fabricated by an IR-fs laser. The high temperature characteristics of silica-based type-II FBGs were tested from 30 to 1100 °C. By analyzing of the data, the formula for the CTE and TOC from 30 °C to 700 °C has been determined. The test values agreed well with the theoretical value at room temperature. Such a hybrid sensor made with IR-fs laser should be a highly promising platform for a variety of high temperature sensing applications.

**Acknowledgments:** The research was supported by Hubei Provincial Natural Science Foundation of China (2015CFA054) and the Open Projects Foundation of Yangtze Optical Fibre and Cable Joint Stock Limited Company (YOFC grant No. SKLD1502).

**Author Contributions:** Litong Li carried out the experiments and wrote the paper; Dajuan Lv finished parts of drawing and writing; Finally, Minghong Yang, Liangming Xiong and Jie Luo reviewed the manuscript.

**Conflicts of Interest:** The authors declare no conflict of interest.

## References

1. Huang, J.Y.; Van, R.J.; Vlekken, J.; Martinez, A.B.; Geernaert, T.; Berghmans, F. FBGs written in specialty fiber for high pressure/high temperature measurement. *Opt. Express* **2017**, *25*, 17936–17947. [[CrossRef](#)] [[PubMed](#)]
2. Zhang, C.; Yang, Y.; Wang, C.; Liao, C.; Wang, Y. Femtosecond-laser-inscribed sampled fiber bragg grating with ultrahigh thermal stability. *Opt. Express* **2016**, *24*, 3981–3988. [[CrossRef](#)] [[PubMed](#)]
3. Bartelt, H.; Elsmann, T.; Habisreuther, T.; Schuster, K.; Rothhardt, M. Optical bragg grating sensor fibers for ultra-high temperature applications. *Proc. SPIE Int. Soc. Opt. Eng.* **2015**, *9655*, 96552S.
4. Bandyopadhyay, S.; Canning, J.; Biswas, P.; Stevenson, M.; Dasgupta, K. A study of regenerated gratings produced in germanosilicate fibers by high temperature annealing. *Opt. Express* **2011**, *19*, 1198–1206. [[CrossRef](#)] [[PubMed](#)]
5. Chikh-Bled, H.; Chah, K.; González-Vila, Á.; Lasri, B.; Caucheteur, C. Behavior of femtosecond laser-induced eccentric fiber bragg gratings at very high temperatures. *Opt. Lett.* **2016**, *41*, 4048–4051. [[CrossRef](#)] [[PubMed](#)]
6. Elsmann, T.; Habisreuther, T.; Graf, A.; Rothhardt, M.; Bartelt, H. Inscription of first-order sapphire bragg gratings using 400 nm femtosecond laser radiation. *Opt. Express* **2013**, *21*, 4591–4597. [[CrossRef](#)] [[PubMed](#)]
7. Qu, S.; Li, Y.; Liu, Y. Single microchannel high-temperature fiber sensor by femtosecond laser-induced water breakdown. *Opt. Lett.* **2013**, *38*, 335–337.
8. Habisreuther, T.; Elsmann, T.; Graf, A.; Schmidt, M.A. High-temperature strain sensing using sapphire fibers with inscribed first-order bragg gratings. *IEEE Photonics J.* **2016**, *8*, 1–8. [[CrossRef](#)]
9. Wang, T.; Shao, L.Y.; Canning, J.; Cook, K. Temperature and strain characterization of regenerated gratings. *Opt. Lett.* **2013**, *38*, 247–249. [[CrossRef](#)] [[PubMed](#)]
10. Habisreuther, T.; Elsmann, T.; Pan, Z.; Graf, A.; Willsch, R.; Schmidt, M.A. Sapphire fiber bragg gratings for high temperature and dynamic temperature diagnostics. *Appl. Therm. Eng.* **2015**, *91*, 860–865. [[CrossRef](#)]
11. Warrensmith, S.C.; Nguyen, L.V.; Lang, C.; Ebendorffheidepriem, H.; Monroe, T.M. Temperature sensing up to 1300 °C using suspended-core microstructured optical fibers. *Opt. Express* **2016**, *24*, 3714–3719. [[CrossRef](#)] [[PubMed](#)]
12. Economidou, S.N.; Karalekas, D. Optical sensor-based measurements of thermal expansion coefficient in additive manufacturing. *Polym. Test.* **2016**, *51*, 117–121. [[CrossRef](#)]
13. Domenegueti, J.F.; Andrade, A.A.; Pilla, V.; Zilio, S.C. Simultaneous measurement of thermo-optic and thermal expansion coefficients with a single arm double interferometer. *Opt. Express* **2017**, *25*, 313–319. [[CrossRef](#)] [[PubMed](#)]
14. Li, C.; Liu, Q.; Peng, X.; Fan, S. Measurement of thermal expansion coefficient of graphene diaphragm using optical fiber Fabry-Perot interference. *Meas. Sci. Technol.* **2016**, *27*, 075102. [[CrossRef](#)]
15. Li, L.T.; Zhang, D.S.; Wen, X.X.; Peng, S.S. FFPI-FBG hybrid sensor to measure the thermal expansion and thermo-optical coefficient of a silica-based fiber at cryogenic temperatures. *Chin. Opt. Lett.* **2015**, *13*, 21–25.
16. Dan, G.; Mihailov, S.J.; Smelser, C.W.; Walker, R.B. Multiparameter sensor based on single high-order fiber bragg grating made with IR-Femtosecond radiation in single-mode fibers. *IEEE Sens. J.* **2008**, *8*, 1223–1228.
17. Li, L.; Tong, X.L.; Zhou, C.M.; Wen, H.Q.; Lv, D.J.; Ling, K. Integration of miniature Fabry-Perot fiber optic sensor with FBG for the measurement of temperature and strain. *Opt. Commun.* **2011**, *284*, 1612–1615. [[CrossRef](#)]
18. Han, Q.; Zhao, X.; Tu, F.; Luo, J. Material composition and structure design in PCVD silica-based single-mode fiber. *Proc. SPIE Int. Soc. Opt. Eng.* **2006**, *6352*, U1300–U1307.
19. Zhang, Q.; Hu, L.; Qi, Y.; Liu, G.; Ianno, N.; Han, M. Fiber-optic refractometer based on a phase-shifted fiber bragg grating on a side-hole fiber. *Opt. Express* **2015**, *23*, 16750–16759. [[CrossRef](#)] [[PubMed](#)]



20. Zhang, Z.J.; Shi, W.K.; Kan, G.; Fang, Z.J. Thermo-optic coefficient and temperature sensitivity of long-period fiber gratings. *Opt. Tech.* **2004**, *30*, 525–528.
21. Yu, Y.; Tam, H.; Chung, W.; Demokan, M.S. Fiber bragg grating sensor for simultaneous measurement of displacement and temperature. *Opt. Lett.* **2000**, *25*, 1141–1143. [[CrossRef](#)] [[PubMed](#)]



© 2018 by the authors. Licensee MDPI, Basel, Switzerland. This article is an open access article distributed under the terms and conditions of the Creative Commons Attribution (CC BY) license (<http://creativecommons.org/licenses/by/4.0/>).